1-1-2015

Contribution of radicals and ions in catalyzed growth of single-walled carbon nanotubes from low-temperature plasmas

Z Marvi
Sahand University of Technology

S Xu
Nanyang Technological University, Singapore

G Foroutan
Sahand University of Technology

Kostya Ostrikov
University of Wollongong

Contribution of radicals and ions in catalyzed growth of single-walled carbon nanotubes from low-temperature plasmas

Abstract

The growth kinetics of single-walled carbon nanotubes (SWCNTs) in a low-temperature, low-pressure reactive plasma is investigated using a multiscale numerical simulation, including the plasma sheath and surface diffusion modules. The plasma-related effects on the characteristics of SWCNT growth are studied. It is found that in the presence of reactive radicals in addition to energetic ions inside the plasma sheath area, the effective carbon flux, and the growth rate of SWCNT increase. It is shown that the concentration of atomic hydrogen and hydrocarbon radicals in the plasma plays an important role in the SWCNT growth. The effect of the effective carbon flux on the SWCNT growth rate is quantified. The dependence of the growth parameters on the substrate temperature is also investigated. The effects of the plasma sheath parameters on the growth parameters are different in low- and high-substrate temperature regimes. The optimum substrate temperature and applied DC bias are estimated to maximize the growth rate of the single-walled carbon nanotubes.

Keywords

growth, single, walled, carbon, nanotubes, low, temperature, contribution, plasmas, radicals, ions, catalyzed

Disciplines

Engineering | Physical Sciences and Mathematics

Publication Details

Marvi, Z., Xu, S., Foroutan, G. & Ostrikov, K. (2015). Contribution of radicals and ions in catalyzed growth of single-walled carbon nanotubes from low-temperature plasmas. Physics of Plasmas, 22 013504-1-013504-10.

Contribution of radicals and ions in catalyzed growth of single-walled carbon nanotubes from low-temperature plasmas

Z. Marvi,[1,2] S. Xu,[2] G. Foroutan,[1] and K. Ostrikov[3]
[1]*Physics Department, Faculty of Science, Sahand University of Technology, 51335-1996 Tabriz, Iran*
[2]*Plasma Sources and Applications Center, NIE, and Institute of Advanced Studies, Nanyang Technological University, 637616 Singapore*
[3]*Institute for Future Environments and School of Chemistry, Physics, and Mechanical Engineering, Queensland University of Technology, Brisbane, QLD 4000, Australia; Plasma Nanoscience Center Australia (PNCA), Manufacturing Flagship, CSIRO, P.O. Box 218, Lindfield, NSW 2070, Australia; Plasma Nanoscience, School of Physics, University of Sydney, Sydney, NSW 2006, Australia; Institute for Superconducting and Electronic Materials (ISEM), University of Wollongong, NSW 2522, Australia; and School of Physics and Advanced Materials, University of Technology Sydney, Sydney, NSW 2006, Australia*

(Received 17 September 2014; accepted 8 December 2014; published online 9 January 2015)

The growth kinetics of single-walled carbon nanotubes (SWCNTs) in a low-temperature, low-pressure reactive plasma is investigated using a multiscale numerical simulation, including the plasma sheath and surface diffusion modules. The plasma-related effects on the characteristics of SWCNT growth are studied. It is found that in the presence of reactive radicals in addition to energetic ions inside the plasma sheath area, the effective carbon flux, and the growth rate of SWCNT increase. It is shown that the concentration of atomic hydrogen and hydrocarbon radicals in the plasma plays an important role in the SWCNT growth. The effect of the effective carbon flux on the SWCNT growth rate is quantified. The dependence of the growth parameters on the substrate temperature is also investigated. The effects of the plasma sheath parameters on the growth parameters are different in low- and high-substrate temperature regimes. The optimum substrate temperature and applied DC bias are estimated to maximize the growth rate of the single-walled carbon nanotubes.
 [http://dx.doi.org/10.1063/1.4905522]

I. INTRODUCTION

In the last decade, low-temperature reactive plasmas have attracted a considerable attention for the controlled synthesis of vertically aligned carbon nanostructures, such as single-walled carbon nanotubes (SWCNTs) and carbon nanofibers (CNFs),[1–13] which are potentially attractive for many applications including nanoelectronics, field emission, nanocomposites, energy storage, sensors, biomedical device, and several others.[14–24]

The significant recent interest in reactive plasmas for materials processing is due to their numerous remarkable characteristics.[25–29] Through the various plasma-chemical reactions, occurring in the gas phase of the plasma, diverse combinations of electrons, ions, and radicals are created. The ions accelerated by the plasma sheath electric field at the plasma-substrate interface accompanied with fluxes of highly reactive radicals towards the substrate provide the required carbon-bearing species for the plasma-based synthesis of high-aspect-ratio carbon nanostructures.

Plasma-enhanced chemical vapor deposition (PECVD) is one of the most versatile plasma-based methods for highly selective synthesis of well-aligned carbon nanostructures. Using the PECVD technique, in addition to vertical growth, the CNTs can be grown at lower temperatures than in the neutral gas-based CVD process, due to the ion and radical-related reactions on the CNT surface.[9,19,20,30]

Catalyst nanoparticles (CNP) play multiple roles in the growth of carbon nanostructures in PECVD. They serve as a growth pattern for SWCNT arrays, activate the surface for CNT nucleation, and help controlling the SWCNT thickness.[1,31–34] In the SWCNT growth, the catalyst particle is located at the base of the nanotube.[15,35,36,39] In this case, each nucleated SWCNT grows on a metal catalyst particle so that the pattern of the nanostructure array repeats the catalyst pattern, which is usually pre-fabricated on the substrate surface.

Apart from the common processes in the CVD growth (adsorption and desorption of radicals, thermal dissociation of hydrocarbon radicals and evaporation of C atoms), there are additional plasma-specific reactions on the SWCNT surface including ion-induced dissociation of adsorbed hydrocarbon species, direct ion decomposition, and etching gas interaction with the adsorbed species, which are responsible for the SWCNT growth at low temperatures. Through this processes, the carbon atoms are created on the SWCNT surface and then diffuse to the nanotube and are finally incorporated into the growing SWCNT via the CNP.

The plasma sheath plays a crucial role in the nanostructure growth processes. Changes in the sheath properties due to variations in the plasma parameters can be used to effectively control the plasma-assisted growth of different nanostructures.[26] The sheath thickness can be controlled by the plasma parameters and directly affects the electric field strength. Consequently, it can be used to control the distribution and kinetic energy of charged species impinging onto the SWCNT surface. In order to control the deposition process and optimize the SWCNT growth parameters, it is necessarily to determine a self-consistent set of the plasma sheath parameters, in particular, to incorporate into the plasma sheath and the surface interaction models.

In recent years, many experimental and numerical studies were devoted to the carbon nanotube and nanofiber growth by PECVD. A surface diffusion model for SWCNT growth was used to obtain the conditions under which a plasma environment can improve the SWCNT growth.[37] Moreover, the growth parameters depend on the catalyst surface temperature, as well as on the ion and etching gas fluxes onto the catalyst nanoparticles.[38] During the initial stage of the nanotube formation on the catalyst nanoparticle patterns,[39] the degree of ionization of the carbon flux strongly affects the kinetics of nanotube and nanocone nucleation. A sheath model was developed to quantify the plasma-sheath-related effects on the CNF growth characteristics.[40] A hybrid molecular dynamics/force-biased Monte Carlo simulations explained the growth mechanism and clarified the chirality formation of SWCNT on a substrate-bound Ni40 cluster.[41] The SWCNT nucleation mechanism on Au catalyst nanoparticles on a Si substrate exposed to the reactive plasma in a $Ar + H_2 + CH_4$ gas mixtures was also reported.[42]

Most of the existing theoretical models of the PECVD growth of SWCNTs rely on a selected adsorbed hydrocarbon radical species or incident ions on the SWCNT surface. As mentioned above, one of the main advantages of the plasma-based growth is the ability to generate highly reactive, dehydrogenated radical species and deliver them to the catalyst particles. Therefore, in order to increase relevance to low-temperature plasma-based nanoscale synthesis experiments, this work considers a multi-component plasma in $Ar + H_2 + CH_4$ mixtures and presents a surface deposition model with multiple adsorbed species linked to the plasma sheath model. Moreover, the effects of each species are compared on the growth parameters. These fundings will help optimizing the generation of relevant radical species in plasma-based nanofabrication experiments.

The paper is organized as follows. In Sec. II, the multiscale numerical model, which involves the electrostatic sheath and surface diffusion model and includes the main assumptions, basic equations, and the applied numerical method, is introduced. Section III presents the results of numerical simulation for the plasma sheath structure and the growth parameters, incident ion and radical fluxes on the SWCNT surface, as well as the plasma sheath-related effects on the SWCNT growth parameters. The paper is concluded in Sec. IV with a summary of the main results.

II. NUMERICAL MODEL AND BASIC EQUATIONS

This section describes a multiscale model that involves the plasma sheath and plasma-surface interaction modules. Figure 1(a) shows the geometry of the plasma sheath formed near a plasma-exposed conductive substrate. The substrate is placed on a substrate-holding platform of temperature T_h. The plasma-sheath boundary is located at $z = 0$, with the plasma sheath filling the half space $z > 0$. The sheath electric field is directed along the z axis and accelerates ion species toward the substrate. Figure 1(b) shows the sketch of a SWCNT with a metal CNP on the base, subjected to the incoming neutral and ionic plasma species from the reactive plasma in an $Ar + H_2 + CH_4$ mixture. The key species that

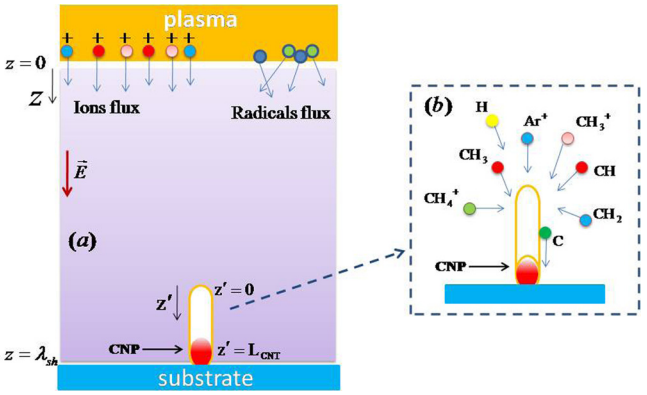

FIG. 1. Schematics of the geometry of the plasma sheath and charged and neutral particles impinging on the CNT and substrate surfaces.

interact with the SWCNT surface are CH, CH_2, CH_3, and H neutral radicals and CH_3^+ and CH_4^+ ions. A conventional fluid model used to investigate the structure of the plasma sheath incorporates electron, positive ion, and radical species. For the electrons and ions, the effects of ionization, collisions with neutrals are considered, but the electron-ion collisions are neglected. It is assumed that the electrons and positive ions have constant temperature throughout the sheath, and radicals have the same temperature with the ions. In the multi-fluid approach, the density and speed of the particles are described by the continuity

$$\frac{d}{dz}(n_i v_i) = \nu_{\text{ion}}^i n_e, \tag{1}$$

$$\frac{d}{dz}(n_e v_e) = \sum_i \nu_{\text{ion}}^i n_e, \tag{2}$$

and momentum equations

$$m_i v_i \frac{dv_i}{dz} = -e\frac{d\phi}{dz} - \frac{T_i}{n_i}\frac{dn_i}{dz} - m_i \nu_g^i v_i, \tag{3}$$

$$0 = e\frac{d\phi}{dz} - \frac{T_e}{n_e}\frac{dn_e}{dz} - m_e \nu_g^e v_e, \tag{4}$$

with $i = Ar^+, CH_4^+, CH_3^+$, where m_j is the mass, n_j is the number density, and v_j is the fluid velocity of the particle species j ($j = i$, e for positive ions and electrons, respectively), and ϕ designates the sheath potential. Moreover, ν_{ion}^i and ν_g^j are the ionization frequency and the collision frequencies of the electrons and positive ions with neutrals, respectively. The Poisson's equation

$$\frac{d^2\phi}{dz^2} = 4\pi\left[e\left(n_e - \sum_i n_i\right)\right] \tag{5}$$

relates the densities of charge particles to the electric potential. The set of Eqs. (1)–(5) is used to investigate the structure of the plasma sheath formed near the substrate. Using the numerical solution of the sheath equations, the positive ions energy and flux and radicals flux (which are the essential parameters in the nanotube growth model) at the substrate are determined.

Here, we introduce the main equations of the plasma-surface interaction in the SWCNT growth model with a CNP on the base. It is assumed that the SWCNT is grown on the top of a CNP which is attached to the substrate at $z' = L_{CNT}$, where z' is a coordinate along the axis of a SWCNT with length L_{CNT}. The SWCNT surface is exposed to the fluxes of incoming radicals (CH, CH_2, CH_3, and H) and positive ions (CH_3^+, and CH_4^+) from the plasma. These fluxes contribute to the growth of the SWCNT on the top of the CNP through surface processes which result in the carbon atoms creation on the SWCNT surface. It is assumed that the carbon atoms created on the SWCNT surface diffuse to the CNT base and then incorporate into the growing CNT wall through the CNP.[43] It is assumed that in the absence of heating effect, the CNP (T_c) and substrate (T_s) temperatures are the same (equal). According to the above assumptions, the main equations of the model are the mass balance equations for CH, CH_2, CH_3, H, and C radicals on the lateral SWCNT surface

$$j_j(1-\theta_t) - \theta_j L_j = 0, \tag{6}$$

$$j_H(1-\theta_t) + \theta_{CH_3} M - \theta_H K = 0, \tag{7}$$

$$D_s \frac{d^2 n_C}{dz'^2} + \sum_j n_j \nu \exp\left(\frac{-E_{tdj}}{k_B T_c}\right) + \sum_i \sum_j \theta_j J_i y_{di} + \sum_i J_i - n_C \nu \exp\left(\frac{-E_{ev}}{k_B T_c}\right) - n_C \sigma_{ads} j_H = 0, \tag{8}$$

where

$$L_j = \sum_j J_i y_{di} + v_0 \sigma_{ads} j_H + v_0 \exp\left(\frac{-E_{dj}}{k_B T_c}\right) + v_0 \exp\left(\frac{-E_{tdj}}{k_B T_c}\right), \tag{9}$$

$$K = v_0 \exp\left(\frac{-E_{dH}}{k_B T_c}\right) + v_0 \sigma_{ads}(P_{Ni} j_H + J_H), \tag{10}$$

$$M = \sum_i J_i y_{di} + v_0 \exp\left(\frac{-E_{td}}{k_B T_c}\right), \tag{11}$$

and indices i and j denote hydrocarbon ions (here, CH_3^+ and CH_4^+) and radicals (here, CH, CH_2, and CH_3), respectively. The first term in Eqs. (6) and (7) accounts for the adsorption of hydrocarbon radicals and H atoms on the SWCNT surface. In Eq. (8), the first, fifth, and sixth terms describe the carbon loss due to surface diffusion, evaporation, and interaction of C with atomic hydrogen from the plasma sheath, respectively. The second, third, and fourth terms in Eq. (8) describe carbon generation due to the thermal and ion-induced dissociation and the decomposition of hydrocarbon radicals. The first, second, third, and fourth terms in the expression for L quantify the hydrocarbon radicals loss due to ion bombardment, interaction with atomic hydrogen from the plasma, desorption, and thermal dissociation, respectively. The first and second terms in Eq. (10) account for desorption and interaction of adsorbed hydrogen atoms with incoming hydrogen atoms (with the probability of P_{Nirec}) and ions from the plasma, respectively. Finally, Eq. (11) describes hydrogen atom generation due to ion induced and thermal dissociation of hydrocarbon molecules. In Eq. (8)

$$D_s = D_{s0} \exp(-E_{sd}/k_B T_c)$$

is the surface diffusion coefficient, where D_{s0} is a diffusion constant.[44]

From Eqs. (6) and (7), the surface coverages by H and hydrocarbon radicals as a function of θ_C are obtained. The following differential equation for surface diffusion of carbon is obtained from Eq. (8)

$$D_s \frac{d^2 n_C}{dz'^2} + F_C - n_C/\tau_a = 0, \tag{12}$$

where $F_C = Q - Q\sum_i J_i/K + \sum_i J_i$ is the effective carbon flux to the SWCNT surface. Here, $Q = [v_0 \nu \exp(-E_{td}/k_B T_c)[1+L_1 J_{CH2}/(L_2 J_{CH}) + L_1 J_{CH3}/(L_3 J_{CH})] + (\sum_i J_i y_{di})[1+(L_1 J_{CH2}/(L_2 J_{CH})) + (L_1 J_{CH3}/(L_3 J_{CH}))]]/[(1+L_1 j_{CH2}/L_2 j_{CH} + L_1 j_{CH3}/L_3 j_{CH} + L_1/j_{CH})K + L_1 j_H/j_{CH} + (ML_1/L_3)(j_{CH3}/j_{CH})]$. The characteristic residence time of carbon atoms on the CNT surface, τ_a, is obtained from following equation:

$$\tau_a = [Q/v_0 + \nu \exp(-E_{ev}/k_B T_c) + \sigma_{ads} j_H]^{-1}. \tag{13}$$

The carbon concentration is obtained from the solution of Eq. (12) with the appropriate boundary conditions. First, it is assumed that $dn_C/dz' = 0$ at the top of CNT ($z' = 0$). Second, it is assumed that $D_s dn_C/dz' = kn_C$ at the CNT base ($z' = L_{CNT}$), where $k = C_k \exp(-\delta E_{inc}/k_B T_c)$ is the incorporation speed, C_k is a constant,[38] and δE_{inc} is the energy barrier for the incorporation of C atoms into the CNT at the base. Taking into account the above boundary conditions, n_C is obtained

$$n_C(z') = F_C \tau_a \left[1 - \frac{\cosh(z'/\lambda_D)}{\cosh(z'/\lambda_D) + (D_s/k\lambda_D)\sinh(z'/\lambda_D)}\right]. \tag{14}$$

Having n_C, the surface diffusion flux of carbon atoms on the CNT wall can be calculated from the following equation:

$$J_s = -D_s \left.\frac{dn_C}{dz'}\right|_{z'=L_{CNT}} \times (2\pi r_p L_{CNT}). \tag{15}$$

Finally, the surface diffusion flux determines the SWCNT growth rate $R_t = m_C J_s/(\pi r_p{}^2 \rho)$, where m_C is the mass of a carbon atom and $\rho \approx 2\text{gcm}^{-3}$ is the CNT material density.

Using a fourth order Runge Kutta method, we have developed a computer code for simulating the sheath region near the substrate in one dimension. The growth kinetics equations include the mass balance equations on the catalyst surface, which are simultaneously solved on the catalyst surface to obtain the growth characteristics such as the carbon surface concentration. The simulation results are consistent with the experimental findings for the SWCNT growth in low-temperature plasmas.

III. NUMERICAL RESULTS AND DISCUSSION

In this section, the numerical solutions of the multiscale model equations are used to determine the dependence of the SWCNT growth parameters (e.g., total SWCNT growth rate, surface coverages of radical species, and effective carbon flux

to the SWCNT surface) on the plasma and substrate parameters. A low-temperature, low-pressure plasma of $Ar + H_2 + CH_4$ gas mixtures is considered. The following parameters are used as a default set: $n_{0e} = 10^{12}\text{cm}^{-3}$, $p_0 = 60\,\text{mTorr}$, $T_e = 1.5\,\text{eV}$, $T_n = T_i = 0.05\,\text{eV}$, $N_{0Ar^+} = 0.6$, $N_{0CH_3^+} = 0.25$, $N_{0CH_4^+} = 0.15$, $u_{0i} = 1.0$, $u_{0e} = 0$, $r_{CH} = 0.2$, $r_{CH_2} = 0.15$, $r_{CH_3} = 0.1$, $r_H = 0.05$, $r_p = 50\,\text{nm}$, $L_{CNT} = 100\,\text{nm}$, $\rho_c = 2\,\text{g cm}^{-3}$, and $\Phi_w = -100$, where N_{0i} and u_{0i} are the ratio of the ion species i to electron density and the Bohm velocity of this species at the sheath edge, respectively. Likewise, r_j (j=H, CH, CH_2, and CH_3) is the ratio of neutral radicals to the total neutral density in the plasma sheath. Also, r_p, L_{CNT}, and ρ_d are the CNP radius, length, and mass density, respectively, whereas Φ_w is the normalized bias potential. The energies associated with all processes considered on the catalyst and SWCNT surfaces are: $E_{td} = 2.1\,\text{eV}$, $E_{bd} = 1.6\,\text{eV}$, $E_{sd} = 0.3\,\text{eV}$, $E_{dCH} = 1.8\,\text{eV}$, $E_{dH} = 1.8\,\text{eV}$, and $E_{ev} = 1.8\,\text{eV}$.

A. Effect of plasma parameters

Here, we focus on the plasma-related effects such as the electron number density at the sheath edge, electron temperature, and the percentages of different hydrocarbon radicals on the ion energy, ion and radical fluxes toward the SWCNT surface, as well as the growth parameters. In Fig. 2, the surface coverages of hydrocarbon radicals and C atoms on the SWCNT surface, effective carbon flux, and the total SWCNT growth rate as a function of plasma bulk electron number density are displayed for three different values of substrate temperature T_s.

It is seen that the surface coverage of C, effective carbon flux, and the total growth rate increase with n_{e0} for all ranges of T_s. Whereas the surface coverages of the hydrocarbon radicals decrease with n_{e0}. This is because, with increasing of the electron number density, the ion fluxes increase due to the more effective ionization. Moreover, as the sheath thickness decreases with n_{e0},[45] the strength of the electric field increases. As a result, the kinetic energy of positive ions also increases.

Figure 3 shows how the ion fluxes and energies change by variation of n_{e0}. It is clearly seen that increasing n_{e0} leads to higher fluxes of more energetic ions impinging on the SWCNT surface. Consequently, ion-induced dissociation and ion decomposition processes on the surface become more effective. These processes dominate carbon species generation under low surface temperature conditions.

As a result, more hydrocarbon radicals are dissociated. It is noteworthy that according to Fig. 2 the surface coverage of CH is reduced with n_{e0}, more than other hydrocarbon surface coverages. Thus, the CH radicals appear to be the major contribution to the SWCNT growth rate.

On the other hand, it can be seen from Fig. 2 that the effective carbon flux and growth rate, first increase with T_s up to the substrate temperature 800 K but then decrease at higher temperatures. To explain this behavior, it is noted that in the low-temperature range $(400\,\text{K} \le T_s \le 800\,\text{K})$, the dominant processes are the ion-induced dissociation, ion decomposition of hydrocarbon radicals, and interaction of adsorbed species with atomic hydrogen from the plasma sheath.

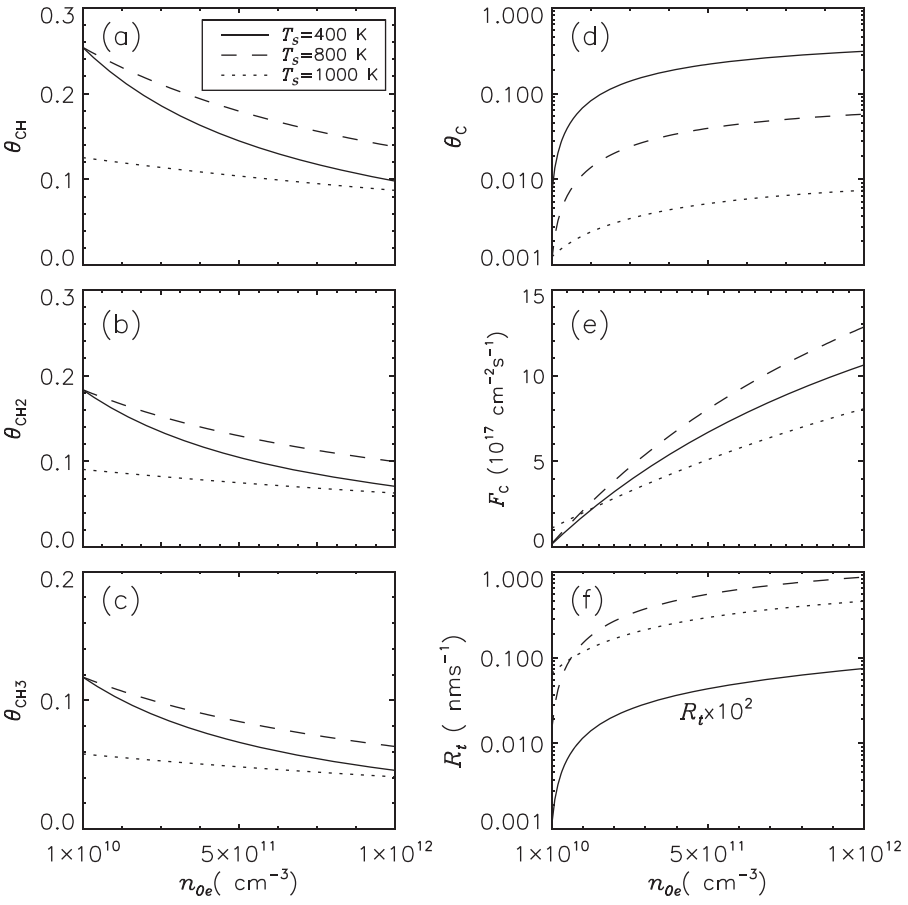

FIG. 2. Profiles of the surface coverage of CH (a), CH_2 (b), CH_3 (c), C (d), effective carbon flux (e), and the growth rate (f), as functions of the electron density at the sheath edge (n_{e0}) for three different values of the substrate temperature. Other parameters in calculation are $T_e = 1.5\,\text{eV}$, $T_i = 0.05\,\text{eV}$, $r_{CH} = 0.2$, $r_{CH_2} = 0.15$, $r_{CH_3} = 0.1$, $r_H = 0.05$, $p_0 = 60\,\text{mTorr}$, and $\Phi_w = -100$.

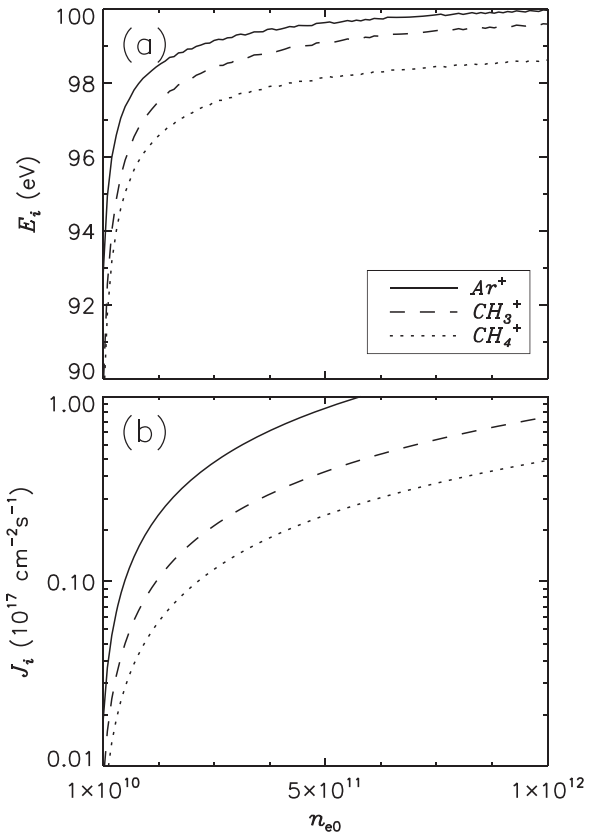

FIG. 3. Dependence of the incident ions energy (a) and flux (b) on the n_{e0}. Other parameters are the same as Fig. 2.

On the other hand, in the high-temperature range ($T_s \geq 800$ K), the processes including adsorption and desorption of the hydrocarbon radicals and atomic hydrogen, thermal dissociation of adsorbed hydrocarbon radicals, desorption of C atoms, and the carbon incorporation into the SWCNT wall through the CNP are the most important processes. Therefore, in the low-temperature PECVD, the ion-induced dissociation and ion decomposition processes are responsible for carbon production.

With increasing T_s, thermal dissociation also leads to carbon creation and as a result increases the effective carbon flux and the growth rate. Moreover, at even higher temperatures, the desorption and evaporation of C atoms lead to significant carbon loss and hence a decrease of the growth rate. We have found that the substrate temperature $T_s \approx 800$ K is a favorable, and may be the optimum temperature for SWCNT growth in PECVD within the parameter range considered here.

Figure 4 shows the effects of the electron temperature on the growth parameters for three different substrate temperatures T_s. It is seen that, while the surface coverage of hydrocarbon radicals decreases, the effective carbon flux and the growth rate increase with T_s. To explain this behavior, it is noted that the flux and kinetic energy of ions at the SWCNT wall both increase with T_s, according to Fig. 5. This leads to the effective ion-induced dissociation and ion decomposition on the SWCNT surface and hence, dramatically decreases the surface coverage of hydrocarbon radicals on the SWCNT surface and increase the carbon production

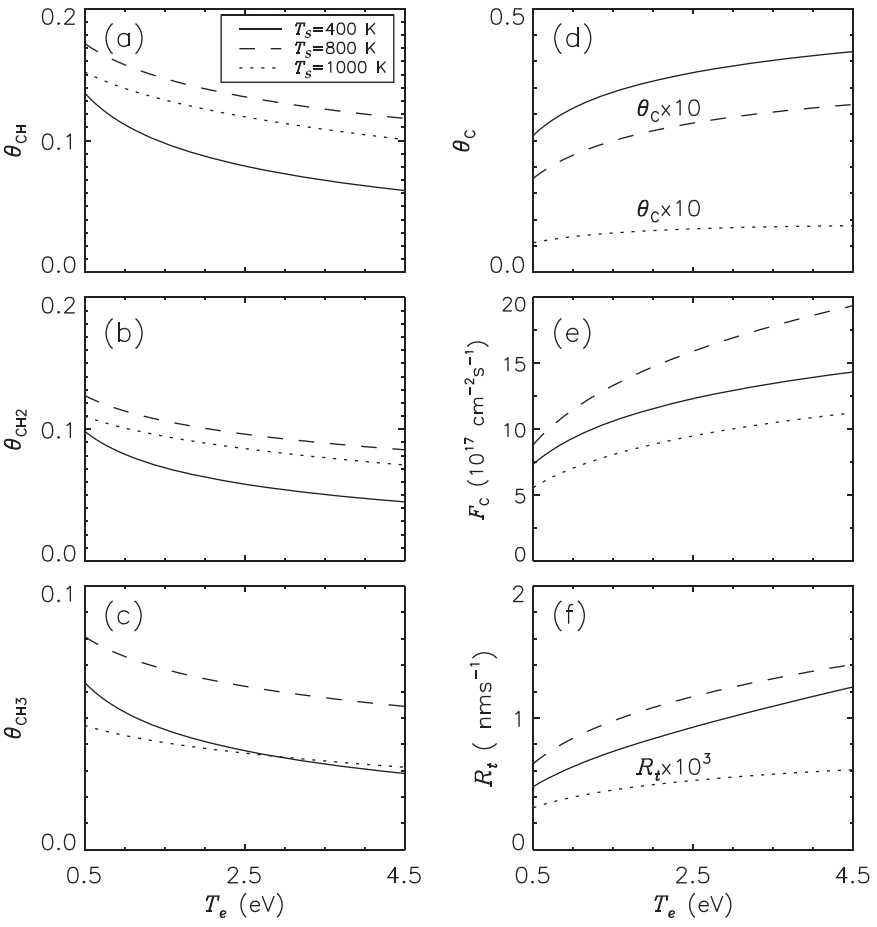

FIG. 4. Profiles of the surface coverage of CH (a), CH_2 (b), CH_3 (c), C (d), effective carbon flux (e), and the growth rate (f), as functions of T_e for three different values of the substrate temperature. Other parameters are the same as Fig. 2.

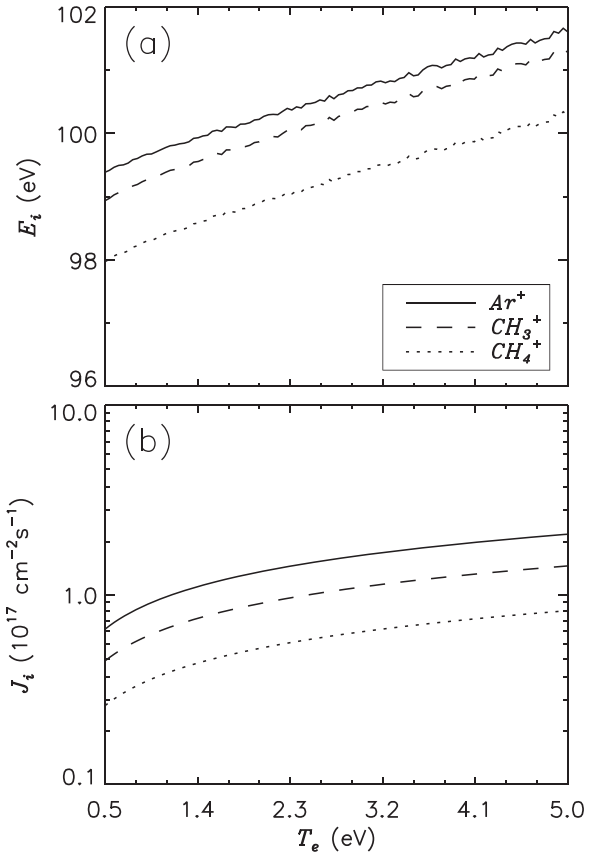

FIG. 5. Dependence of the incident ions energy (a) and flux (b) on the T_e. Other parameters are the same as Fig. 2.

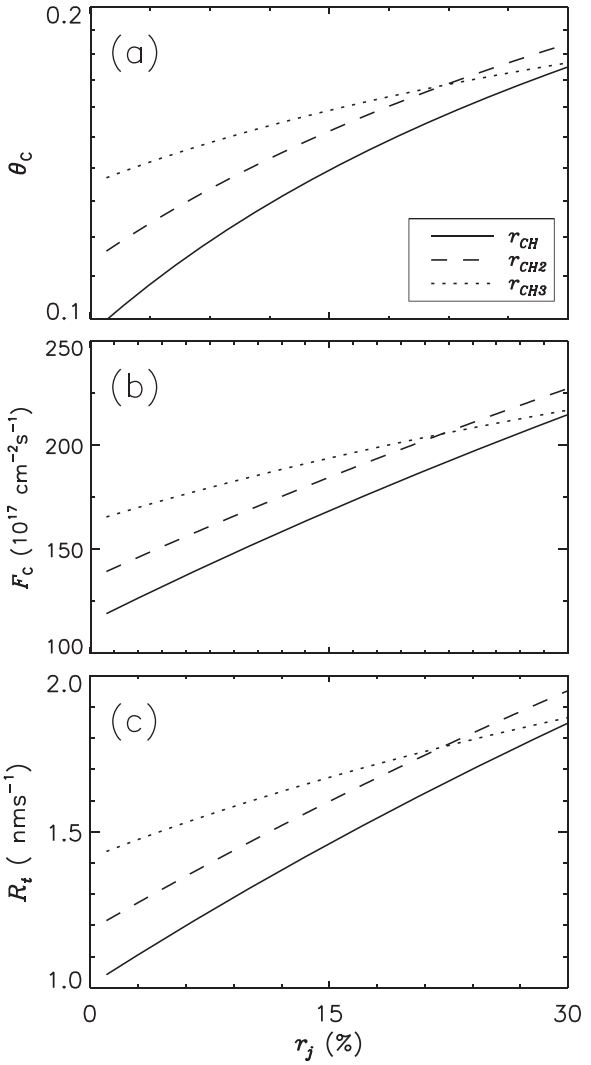

FIG. 6. Profiles of the surface coverage of C (a), effective carbon flux (b), and total growth rate (c), as functions of r_{CH} (solid), r_{CH_2} (dashed), and r_{CH_3} (dotted). Other parameters are the same as Fig. 2.

on the SWCNT surface, as well as the effective carbon flux and growth rate. Moreover, a higher electron temperature leads to expanding of the sheath width. This is why the energy of ions (upon impacting on the SWCNT surface) and the ion fluxes deposited on the SWCNT surface increase.

Let us turn our attention to the effects of different hydrocarbon radicals on the SWCNT growth. Figure 6 presents the surface coverages of carbon, the effective carbon flux, and the growth rate as a function of the relative concentrations of three different hydrocarbon radicals (r_j). The carbon surface coverage, effective carbon flux, as well as the growth rate increase with r_j. The increase is more pronounced when the percentage of CH radical is increased compared to other radical species.

B. Effects of other process parameters

To explore the effects of total gas pressure p_0 on the growth parameters of SWCNT, we first calculated the influence of p_0 on the ion and neutral fluxes and ion energies. Figure 7 shows the dependence of the deposited ion and radical fluxes, and ion energies on p_0. It is found that the incident flux of the hydrocarbon ions is independent of the total gas pressure, while the hydrocarbon radicals flux is significantly enhanced with p_0. The kinetic energy of incident ions into the SWCNT surface is reduced with p_0 (as can be seen from Fig. 7(a)).

To explain these results we note that with increasing p_0 and hence the gas number density (it is assumed that the neutral temperature is constant), more hydrocarbon, and hydrogen ions and radicals are produced through the electron impact reactions. On the other hand, the sheath becomes wider with increasing p_0, which then leads to a reduction of the electric field inside the sheath, as well as lower ion velocities onto the substrate. Consequently, increasing the total pressure is accompanied with an increase in the ion density and a decrease in the ion velocity. All these changes lead to the higher fluxes of radicals on the SWCNT surface, while the ion fluxes remain nearly constant.

To study the pressure variation effects in the presence of different radical species on the SWCNT growth process, the surface coverages of H and C atoms, effective carbon flux, and SWCNT growth rate are plotted in Fig. 8, as a function of total gas pressure for four different cases of the radical species concentration inside the plasma sheath (we refer to the case of one radical CH, two radicals CH and CH_2, two radicals CH and CH_3, and all three hydrocarbon radicals CH, CH_2, and CH_3 as a case I, II, III, and IV, respectively). It is found that the carbon surface coverage, effective carbon flux, and the growth rate all increase with p_0 in all cases.

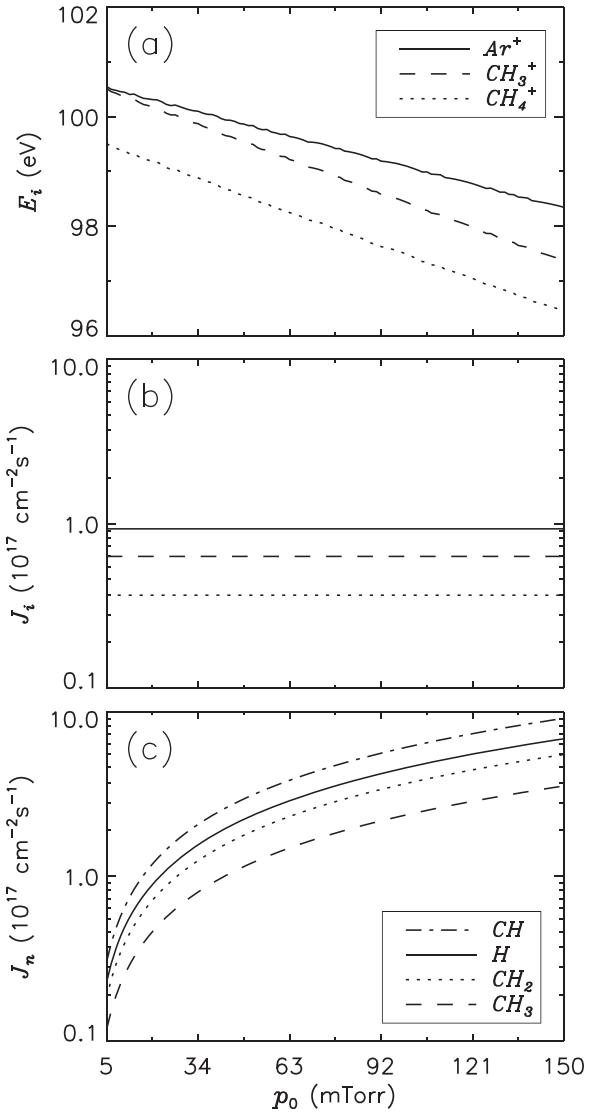

FIG. 7. Dependence of the incident ion energy (a) and flux (b) and neutral radicals flux (c) on the total gas pressure (p_0). Other parameters are the same as Fig. 2.

As mentioned above, both the loss and production of C atoms are enhanced with p_0. However, at the substrate temperature considered here ($T_s = 800$ K), the thermal dissociation of hydrocarbon molecules is more effective than the ion-related processes. In this case, the generation of C atoms can be more likely attributed to the thermal dissociation of hydrocarbon molecules which is also more dominant at high pressures. This is why the carbon surface coverage and SWCNT growth rate increase with p_0. On the other hand, it can be seen from Fig. 8 that the effective carbon flux and the growth rate increase for the case IV rather than the case I. Moreover, from comparison of two cases II and III, it can be deduced that the CH_2 radical species are more effective than CH_3 ones in increasing the growth rate.

The DC applied bias plays an essential role in the control of the ions kinetic energy and distribution on the SWCNT surface. To investigate the effects of the substrate potential (V_{dc}) on the growth parameters, Fig. 9 shows the surface coverage of radicals, effective carbon flux, and the growth rate as a function of the bias potential ($|V_{dc}|$) for three different contributions of the hydrocarbon ion species inside the plasma sheath. It is seen that the surface coverage of carbon atoms, carbon effective flux, and growth rate all increase with $|V_{dc}|$, so that the increase is more effective when both CH_3^+ and CH_4^+ ions are present inside the sheath (see solid curves in Fig. 9).

When the bias potential at the conductive substrate is raised, all of the hydrocarbon ions obtain more kinetic energy due to a stronger electric field. As a result, the ion decomposition and ion-induced dissociation are enhanced, which in turn leads to the surface coverages of hydrocarbon radicals decrease with $|V_{dc}|$. It can be seen from Fig. 9 that the effective carbon flux and SWCNT growth rate increase in the presence of hydrocarbon ions in the sheath. Also, it is noted from Fig. 9 that the growth parameters profiles exhibit a nonlinear dependence on $|V_{dc}|$. Initially, θ_C, F_C, and R_t increase quickly with the $|V_{dc}|$ up to $|V_{dc}| \approx 100$ eV but then they change quite slowly and finally become almost constant at the higher potential. This behavior is prominent for the case when both hydrocarbon ions are present in the sheath. Moreover, by comparing the dashed and dotted lines in Fig. 9, one can find that the CH_3^+ ions provide more contribution in the increase of the growth rate due to higher flux and energy than CH_4^+ ions.

To determine the consumption or production flux of the each neutral species, which participates into the growth process of SWCNT, the effective sticking coefficients β has been calculated. It is defined as a fraction of the incoming flux of the neutral species and is determined by solving the mass balance equation in the interface between the plasma and the substrate surface.[46] Figure 10 shows the calculated effective sticking coefficients as a function of $|V_{dc}|$ for different gas pressures. The effective sticking coefficients of CH_4 and H_2 present the negative values, because these species are products of the surface deposition processes on the SWCNT surface. On the contrary, the effective sticking coefficients of CH_3, CH_2, CH, and H adsorbed species have positive values, because they are being incorporated into the growing SWCNT. It can be seen from Fig. 10 that the sticking coefficients of CH, CH_2, and CH_3 increase with $|V_{dc}|$, whereas all of them decrease with increasing p_0.

IV. SUMMARY AND CONCLUSIONS

Using the multi-scale model, which includes the plasma sheath model coupled with a surface diffusion model, the kinetics of SWCNT growth on the biased substrate in a low-temperature low-pressure plasma reactor is studied. The sheath structure is modeled using a multi-fluid model, which involves electrons, two positive ion, and four reactive radical species. The microenergetic surface diffusion model is based on the mass balance equations for radical species on the SWCNT surface. The effect of the plasma parameters including the bulk electron density, electron temperature, relative concentrations of different radicals, as well as process control parameters such as the total gas pressure, bias potential, and substrate temperature on the ion energies, ion and radical fluxes, and the growth parameters are investigated.

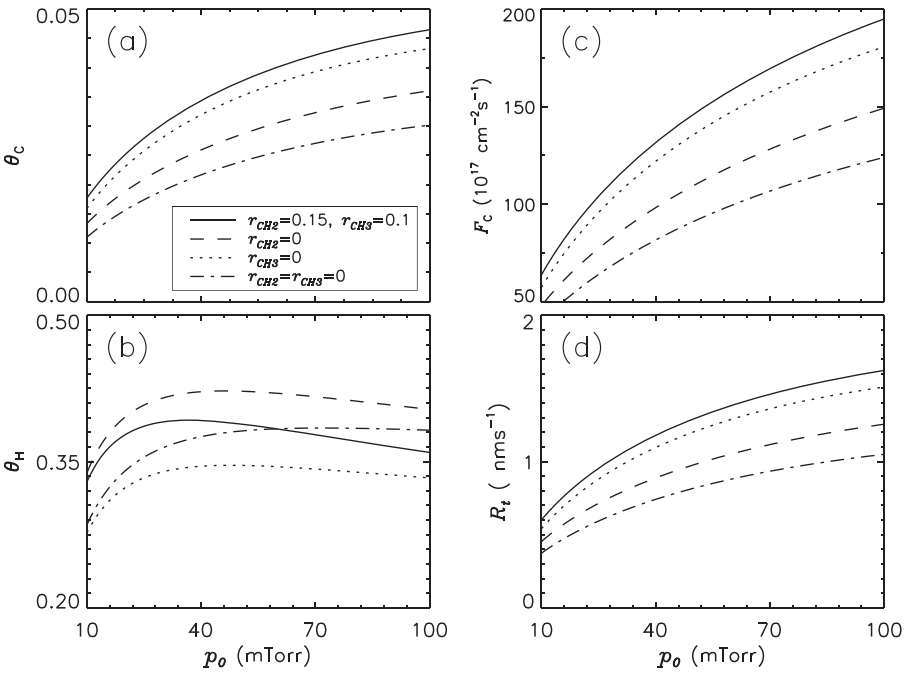

FIG. 8. Profiles of the surface coverage of C (a) and H (b), effective carbon flux (c), and the growth rate (d), as functions of p_0 for different cases of the radical species concentration inside the plasma sheath. Other parameters are the same as Fig. 2.

The results showed that considering two radicals CH and CH_2 in addition to CH_3 in the plasma-surface interaction can improve the growth process. The effective carbon flux and the SWCNT growth rate are computed in this case. Furthermore, the positive ion fluxes and energies as well as the growth rate are shown to increase with the bulk electron number density and temperature. Moreover, the growth parameters show the strong dependence on the substrate

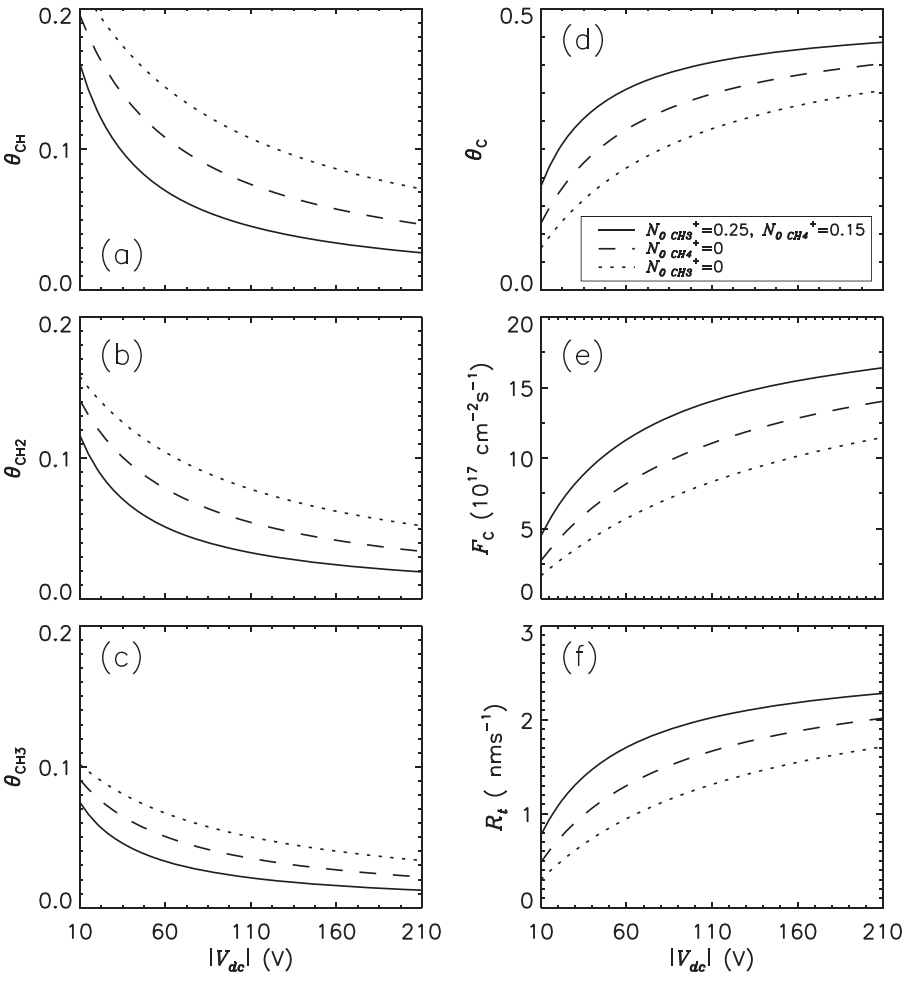

FIG. 9. Profiles of the surface coverage of CH (a), CH_2 (b), CH_3 (c), C (d), and H (e), uncovered surface (f), effective carbon flux (g), and the growth rate (h), as functions of $|V_{dc}|$ for three different contributions of the hydrocarbon ions inside the plasma sheath. Other parameters are the same as Fig. 2.

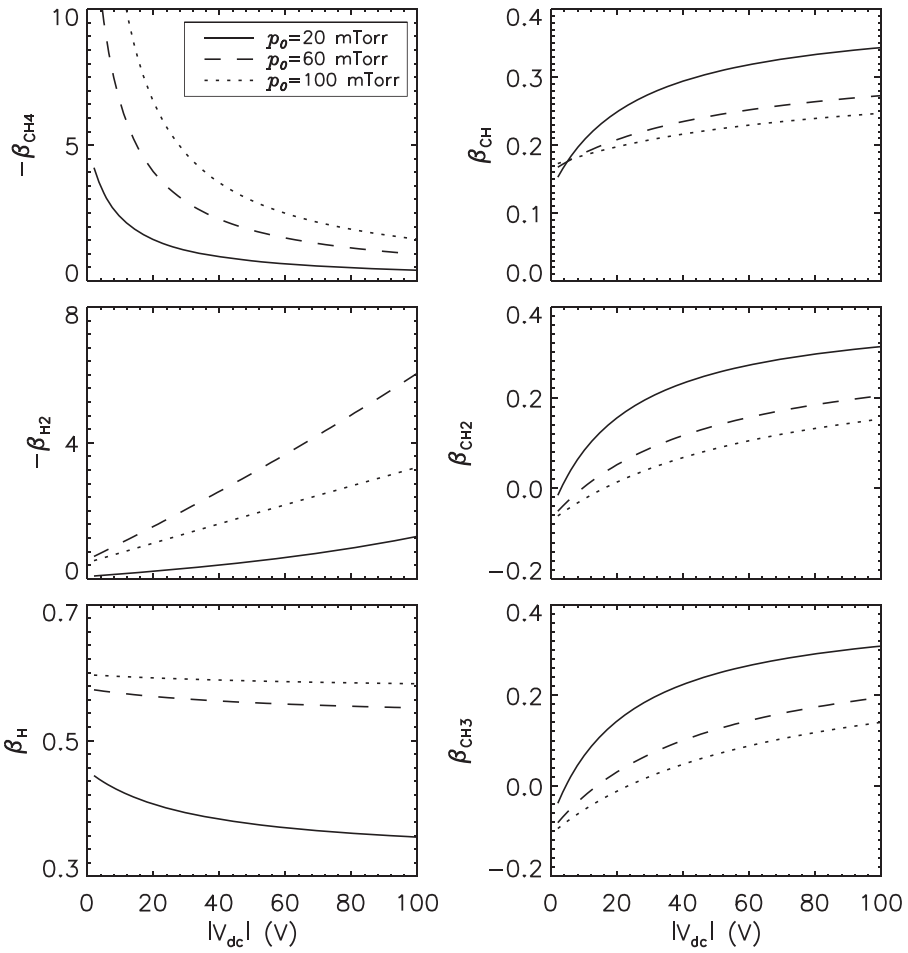

FIG. 10. Sticking coefficient of neutral species as a function of $|V_{dc}|$ for different gas pressures. Other parameters are the same as Fig. 2.

temperature. It is also found that the substrate temperature of 800 K is a favorable temperature for obtaining the maximum growth rate of the single-walled carbon nanotubes.

The ion energies decrease with increasing the total gas pressure due to the increase in the sheath width. However, due to stronger radical fluxes with p_0, the thermal dissociation of radical species enhances the effective carbon flux on the SWCNT substrate. As a result, the growth rate increases with p_0 at the substrate temperatures about 800 K. On the other hand, with increasing DC bias, the effective carbon flux and the growth rate, first increase quickly but then become nearly constant at the higher potential.

The results showed that to maximize the growth rate, $|V_{dc}| \approx 100$ eV is an appropriate DC bias potential which also prevents C atoms accumulation on the CNT surface. The results of this work are relevant to the development of effective and energy-efficient nanotechnologies based on thermally non-equilibrium low-temperature plasmas generated in low-pressure gas discharges.

ACKNOWLEDGMENTS

This work was partially supported by Academic Research Fund (ACRF) Tier 1 (RP 6/13 XS, Singapore), A*STAR (Singapore), the Ministry of Science, Research and Technology of Iran, CSIRO CEO Science Leadership program and the Australian Research Council. The authors wish to thank Dr. Chan Chia Sern and Mr. Mark Lim of PSAC and Dr. Song Dengyuan of Yingli Solar for their valuable comments and discussions on this work.

[1]S. Hofmann, G. Czanyi, A. C. Ferrari, M. C. Payne, and J. Robertson, Phys. Rev. Lett. **95**, 036101 (2005).
[2]I. Levchenko, K. Ostrikov, M. Keidar, and S. Xu, Appl. Phys. Lett. **89**, 033109 (2006).
[3]T. Nozaki, K. Ohnishi, K. Okazaki, and U. Kortshagen, Carbon **45**, 364 (2007).
[4]K. Ostrikov, Rev. Mod. Phys. **77**, 489 (2005).
[5]M. Meyyappan, J. Phys. D: Appl. Phys. **42**, 213001 (2009).
[6]T. Mizutan, H. Ohnaka, Y. Okigawa, S. Kishimoto, and Y. Ohno, J. Appl. Phys. **106**, 073705 (2009).
[7]M. Mao and A. Bogaerts, J. Phys. D: Appl. Phys. **43**, 205201 (2010).
[8]S. Vizireanu, S. D. Stoica, C. Luculescu, L. C. Nistor, B. Mitu, and G. Dinescu, Plasma Sources Sci. Technol. **19**, 034016 (2010).
[9]M. I. Ionescu, Y. Zhang, R. Li, and X. Sun, Appl. Surf. Sci. **258**, 1366 (2011).
[10]E. C. Neyts, J. Vac. Sci. Technol., B **30**, 30803 (2012).
[11]E. C. Neyts, K. Ostrikov, Z. J. Han, S. Kumar, A. C. T. van Duin, and A. Bogaerts, Phys. Rev. Lett. **110**, 065501 (2013).
[12]S. Kumar, H. Mehdipour, and K. Ostrikov, Adv. Mater. **25**, 69 (2013).
[13]K. Ostrikov, J. Phys. D: Appl. Phys. **47**, 224009 (2014).
[14]S. Xu, S. Y. Huang, I. Levchenko, H. P. Zhou, D. Y. Wei, S. Q. Xiao, L. X. Xu, and W. S. Yan, Adv. Energy Mater. **1**, 373 (2011).
[15]M. Keidar, Y. Raitses, A. Knapp, and A. M. Waas, Carbon **44**, 1022 (2006).
[16]S. Xu, H.-S., Li, Y.-a. Li, S. Lee, and C. H. A. Huan, Chem. Phys. Lett. **287**, 731 (1998).
[17]K. N. Ostrikov, I. B. Denysenko, S. Xu, and R. G. Storer, J. Appl. Phys. **92**, 4935 (2002).

[18]K. Ostrikov and A. B. Murphy, J. Phys. D: Appl. Phys. **40**, 2223 (2007).
[19]A. V. Melechko, R. Desikan, T. E. McKnight, and P. D. Klein, J. Phys. D: Appl. Phys. **42**, 193001 (2009).
[20]D. B. Peckys, A. V. Melechko, M. L. Simpson, and T. E. Mcknight, Nanotechnology **20**, 145304 (2009).
[21]C. Liu, F. Li, L. P. Ma, and H. M. Cheng, Adv. Mater. **22**, E28 (2010).
[22]I. Levchenko, S. Y. Huang, K. Ostrikov, and S. Xu, Nanotechnology **21**, 025605 (2010).
[23]X. Li, Y. Jia, J. Wei, H. Zhu, K. Wang, D. Wu, and A. Cao, ACS Nano **4**, 2142 (2010).
[24]Z. L. Wang, R. Guo, G. R. Li, H. L. Lu, Z. Q. Liu, F. M. Xiao, M. Zhang, and Y. X. Tong, J. Mater. Chem. **22**, 2401 (2012).
[25]K. Ostrikov, H. J. Yoon, A. E. Rider, and S. V. Vladimirov, Plasma Processes Polym. **4**, 27 (2007).
[26]K. Ostrikov, E. C. Neyts, and M. Meyyappan, Adv. Phys. **62**, 113 (2013).
[27]X. X. Zhong, X. Wu, and K. Ostrikov, Plasma Processes Polym. **6**, 161 (2009).
[28]L. Yuan, X. X. Zhong, I. Levchenko, Y. Xia, and K. Ostrikov, Plasma Processes Polym. **4**, 612 (2007).
[29]D. Mariotti and R. M. Sankaran, J. Phys. D: Appl. Phys. **43**, 323001 (2010).
[30]J. D. Fowlkes, B. L. Fletcher, S. T. Retterer, A. V. Melechko, M. L. Simpson, and M. J. Doktycz, Nanotechnology **19**, 415301 (2008).
[31]J. C. Charlier, H. Amara, and Ph. Lambin, ACS Nano **1**, 202 (2007).
[32]F. Ding, A. R. Harutyunyan, and B. I. Yakobson, Proc. Natl. Acad. Sci. U.S.A. **106**, 2506 (2009).
[33]Z. Ghorannevis, T. Kato, T. Kaneko, and R. Hatakeyama, J. Am. Chem. Soc. **132**, 9570 (2010).
[34]R. M. Sankaran, J Phys. D.: Appl. Phys. **44**, 174005 (2011).
[35]S. Reich, L. Li, and J. Robertson, Chem. Phys. Lett. **421**, 469 (2006).
[36]S. Hofmann, R. Sharma, C. Ducati, G. Du, C. Mattevi, C. Cepek, M. Cantoro, S. Pisana, A. Parvez, F. Cervantes-Sodi, A. C. Ferrari, R. Dunin-Borkowski, S. Lizzit, L. Petaccia, A. Goldoni, and J. Robertson, Nano Lett. **7**, 602 (2007).
[37]I. Denysenko, K. Ostrikov, M. Y. Yu, and N. A. Azarenkov, J. Appl. Phys. **102**, 074308 (2007).
[38]I. Denysenko, K. Ostrikov, U. Cvelbar, M. Mozetic, and N. A. Azarenkov, J. Appl. Phys. **104**, 073301 (2008).
[39]I. Levchenko, K. Ostrikov, D. Mariotti, and A. B. Murphy, J. Appl. Phys. **104**, 073308 (2008).
[40]H. Mehdipour, K. Ostrikov, and A. E. Rider, Nanotechnology **21**, 455605 (2010).
[41]E. C. Neyts, A. C. T. van Duin, and A. Bogaerts, J. Am. Chem. Soc. **133**, 17225 (2011).
[42]K. Ostrikov and H. Mehdipour, J. Am. Chem. Soc. **134**, 4303 (2012).
[43]O. A. Louchev, T. Laude, Y. Sato, and H. Kanda, J. Chem. Phys. **118**, 7622 (2003).
[44]I. Denysenko and K. Ostrikov, Appl. Phys. Lett. **90**, 251501 (2007).
[45]Z. Marvi and G. Foroutan, Thin Solid Films **550**, 381 (2014).
[46]N. V. Mantzarisa, E. Gogolides, A. G. Boudouvis, A. Rhallabi, and G. Turban, J. Appl. Phys. **79**, 3718 (1996).